

AFOSR-TR- 81-0495

ADA101123

LEVEL

5

SGI-R-80-034

TIME DOMAIN WAVEFORM INVERSION OF SHORT-PERIOD P-WAVES
FOR NUCLEAR EXPLOSION SOURCE TIME FUNCTIONS

LARRY J. RUFF

TECHNICAL REPORT

SPONSORED BY

ADVANCED RESEARCH PROJECTS AGENCY (DoD)

ARPA ORDER No. 3291-21

MONITORED BY AFOSR UNDER CONTRACT #F49620-79-C-0012

DMC FILE COPY

The views and conclusions contained in this document are those of the authors and should not be interpreted as necessarily representing the official policies, either expressed or implied, of the Defense Advanced Research Projects Agency or the United States Government.

January 9, 1981



SIERRA GEOPHYSICS, INC.

150 N. SANTA ANITA AVENUE • ARCADIA, CALIFORNIA 91006 • (213) 574-7052

81 7 06 032

Approved for public release;
distribution unlimited.

ARPA Order: 3291-32

Program Code: 9F10

Effective Date of Contract: October 1, 1978

Contract Expiration Date: September 30, 1980

Amount of Contract: \$444,995

Contract No. F49620-79-C-0012

Principal Investigator and Phone No.:

Dr. Robert S. Hart

(213) 574-7052

Program Manager and Phone No.:

Mr. William J. Best

(202) 767-4908

UNCLASSIFIED
SECURITY CLASSIFICATION OF THIS PAGE (When Data Entered)

REPORT DOCUMENTATION PAGE		READ INSTRUCTIONS BEFORE COMPLETING FORM
1. REPORT NUMBER AFOSR-TR-81-0495	2. GOVT ACCESSION NO. AD-A101123	3. RECIPIENT'S CATALOG NUMBER
4. TITLE (and Subtitle) TIME-DOMAIN WAVEFORM INVERSION OF SHORT-PERIOD P-WAVES FOR NUCLEAR EXPLOSION SOURCE TIME FUNCTIONS	5. TYPE OF REPORT & PERIOD COVERED Final	
7. AUTHOR(s) Larry J Ruff	6. PERFORMING ORG. REPORT NUMBER F49620-79-C-0012	
9. PERFORMING ORGANIZATION NAME AND ADDRESS Sierra Geophysics, Inc. 150 N. Santa Anita Avenue Arcadia, CA 91006	10. PROGRAM ELEMENT, PROJECT, TASK AREA & WORK UNIT NUMBERS A.0.3291-32 9F10	
11. CONTROLLING OFFICE NAME AND ADDRESS DARPA/NMR 1400 Wilson Blvd. Arlington, VA 22209	12. REPORT DATE 9 Jan 81	
14. MONITORING AGENCY NAME & ADDRESS(if different from Controlling Office) AFOSR/NP Bolling AFB Wash DC 20332	13. NUMBER OF PAGES 42	
16. DISTRIBUTION STATEMENT (of this Report) Approved for public release; distribution unlimited.	15. SECURITY CLASS. (of this report) unclassified	
17. DISTRIBUTION STATEMENT (of the abstract entered in Block 20, if different from Report)	15a. DECLASSIFICATION DOWNGRADING SCHEDULE	
18. SUPPLEMENTARY NOTES		
19. KEY WORDS (Continue on reverse side if necessary and identify by block number)		
20. ABSTRACT (Continue on reverse side if necessary and identify by block number) This research investigates the estimation of the source time parameters of underground nuclear explosions from the waveforms of short-period teleseismic P-waves. In the simplest consideration, and when the source yield is unconstrained, there are only three source parameters, two that describe the source time function and one for the delay time of the (p)P phase. There are, of course, indications that the (p)P arrival may not have the same amplitude or shape as the direct P arrival, presumably due to anelastic or nonlinear effects		

UNCLASSIFIED

SECURITY CLASSIFICATION OF THIS PAGE (If *None* Data Entered)

between the shot point and the surface. Thus, we will also consider the effect on the waveforms of a decreased $(p)P$ amplitude. Another parameter which has a significant influence upon the observed waveforms is t (t = travel time/ $Q(av)$). Accordingly, the variation in the source parameter estimates due to a varying t will also be addressed.

UNCLASSIFIED

SECURITY CLASSIFICATION OF THIS PAGE (If *None* Data Entered)



Sierra Geophysics, Inc.

150 N. Santa Anita Ave. • Suite 880 • Arcadia, California 91006 • (213) 574-7052

14 SGI-R-80-034

6

TIME DOMAIN WAVEFORM INVERSION OF SHORT-PERIOD P-WAVES
FOR NUCLEAR EXPLOSION SOURCE TIME FUNCTIONS.

10 LARRY J. RUFF

9 TECHNICAL REPORT

SPONSORED BY

ADVANCED RESEARCH PROJECTS AGENCY (DOD)

ARPA ORDER No. 3291-21

18 AFOSR

19 TR-81-0495

MONITORED BY AFOSR UNDER CONTRACT AF49620-79-C-0012,
15 //ARPA Order-3291

The views and conclusions contained in this document are
those of the authors and should not be interpreted as necessarily
representing the official policies, either expressed or implied,
of the Defense Advanced Research Projects Agency or the United
States Government.

11 9 Jan [REDACTED] 81

12 43

AIR FORCE OFFICE OF SCIENTIFIC RESEARCH (AFSC)
NOTICE OF TRANSMITTAL TO DDC
This technical report has been reviewed and is
approved for public release IAW AFR 190-12 (7b).
Distribution is unlimited.

A. D. BLOSE
Technical Information Officer

393 821 *not*

TABLE OF CONTENTS

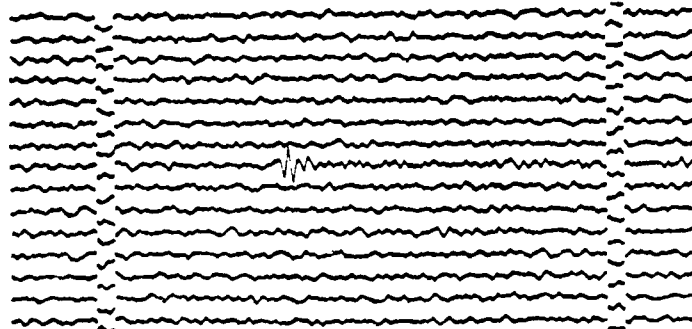
	<u>Page</u>
I. INTRODUCTION.	1
II. METHOD.	8
III. RESULTS	14
3.1 Properties of the Inversion Method	14
3.2 Source Errors Due to Improper t^* and p^p Amplitude	21
3.3 Results for Western Kazakh Test Site . . .	26
3.4 Inversion Using SRO Short-Period Instruments.	29
REFERENCES.	40

Accession For	
NTIS GRA&I	<input checked="" type="checkbox"/>
DTIC TAB	<input type="checkbox"/>
Unannounced	<input type="checkbox"/>
Justification	
By _____	
Distribution/ _____	
Availability Codes _____	
Avail and/or Dist	Special
<i>A</i>	

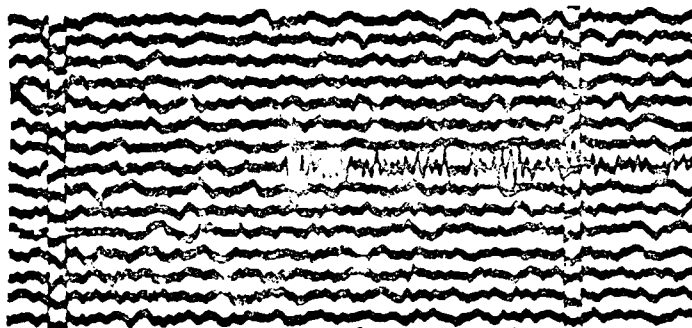
I. INTRODUCTION

This report investigates the estimation of the source time parameters of underground nuclear explosions from the waveforms of short-period teleseismic P-waves. In the simplest consideration, and when the source yield is unconstrained, there are only three source parameters, two that describe the source time function and one for the delay time of the pP phase. There are, of course, indications that the pP arrival may not have the same amplitude or shape as the direct P arrival, presumably due to anelastic or non-linear effects between the shot point and the surface. Thus, we will also consider the effect on the waveforms of a decreased pP amplitude. Another parameter which has a significant influence upon the observed waveforms is t^* ($t^* = \text{travel time}/Q_{av}$). Accordingly, the variation in the source parameter estimates due to a varying t^* will also be addressed.

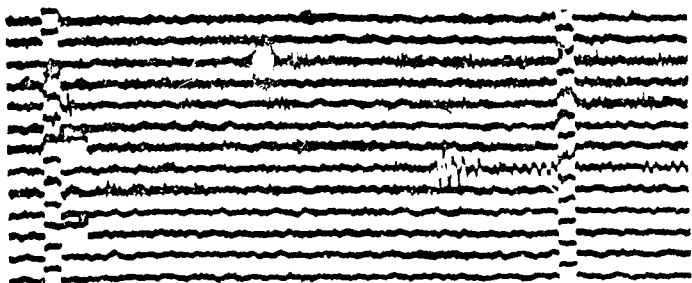
There are other phenomena which can influence the waveforms, such as converted phases at the source and receiver, of which the latter seems to be the most important. We hope to minimize this "noise" principally by selecting "clean" stations when modeling the data. Figure 1 shows a few representative seismograms of underground nuclear events, and the characteristic waveshape that is recorded by short period instruments is evident. Also notice that the seismograms differ substantially from station to station after the first two seconds.



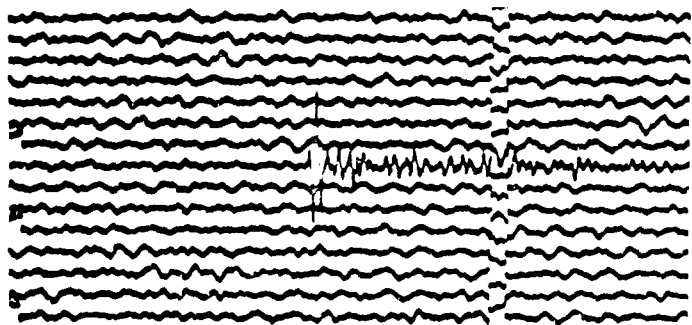
ATL
12-6-69
Mag = 50,000



DUG
12-6-69
Mag = 200,000



GEO
12-6-69
Mag = 25,000



SCP
12-6-69
Mag = 50,000

Figure 1. Representative WWSSN short period seismograms for an event in Western Kazakh, Soviet Union. The time scale is one minute between time marks.

Before discussing the details of determining the source time function, it is useful to review the source representation used. Based on near-field observations, Haskell (1967) introduced a simple analytical formula for the source displacement potential time history, with the condition that acceleration at the source is continuous. Figure 2 is taken from Haskell (1967), and shows the observations and Haskell's analytical function. The far-field time function is basically the time derivative of the near-field potential, dropping the terms which do not propagate to teleseismic distances. Haskell's representation can be expressed in analytical form as:

$$\frac{\psi(t)}{\psi(\infty)} = 1 - e^{-kt} \left(1 + kt + \frac{(kt)^2}{2} + \frac{(kt)^3}{6} - b(kt)^4 \right)$$

There are two parameters present, the time constant k which is proportional to the reciprocal of the far-field rise time, and the overshoot parameter b which characterizes the amount of overshoot, as seen in Figure 2. Von Seggern and Blanford (1972) revised the Haskell source description by allowing the near-field velocity to be discontinuous, and obtained the subsequent analytical expression:

$$\frac{\psi(t)}{\psi(\infty)} = 1 - e^{kt} (1 + kt - B(kt)^2)$$

where once again k is a reciprocal time constant and B characterizes the overshoot. As the von Seggern and Blan-

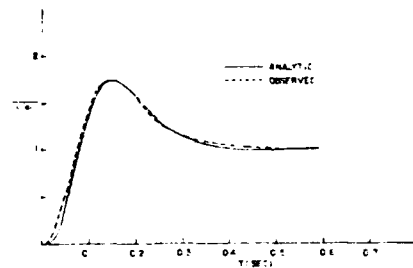


Fig. 2a. Granite.

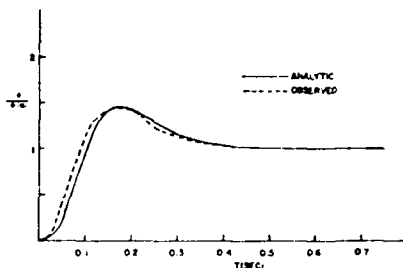


Fig. 2b. Salt

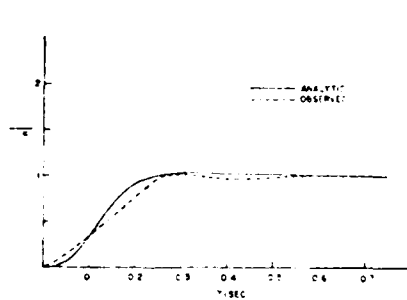


Fig. 2c. Tuff.

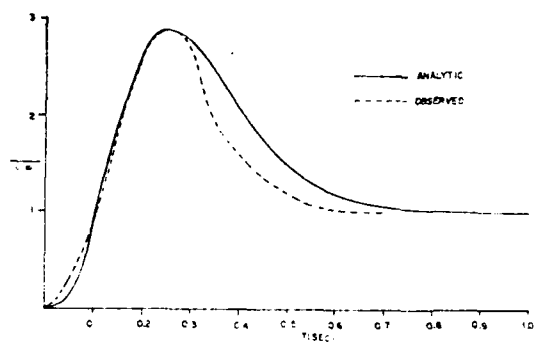


Fig. 2d. Alluvium.

Figure 2 shows the comparison of observed and analytic potentials for 5 kt.

Figure 2. From Haskell (1967).

ford form appears to be consistent with teleseismic spectra, this form will be used throughout.

As indicated by Haskell from a simple scaling argument, k should scale as $Y^{-1/3}$ where Y is the explosion yield, and B is expected to be fairly constant for a particular rock unit. Fitting the von Seggern-Blanford form to the data in Figure 2, the value of k for the 5 kt. explosions varies from ~ 8 to ~ 16 . Accepting the scaling relation for k , an event of 100 kt. size in those materials would give k in the range ~ 3 to ~ 6 . With a more sophisticated scaling law, von Seggern and Blanford used $k = 16.8$ at $Y = 5$ kt. and predicted that $k = 9.6$ at $Y = 80$ kt., while the simple $Y^{-1/3}$ scaling would give $k = 6.7$ for $Y = 80$ kt.

As seen in Figure 2, the amount of overshoot is different for each event. The value of B varies as: ~ 0 for the event in tuff, ~ 2 for the event in granite, and ~ 3.3 for the event in alluvium. It is commonly assumed that the value for B is mostly dependent upon the rock type containing the explosion and does not depend strongly on explosion yield. Placing an upper limit on the B value from knowledge of the containment rock would be a useful constraint in deducing the source parameters, as will be seen later.

The delay time of the surface reflection is dependent on rock type and depth of burial. For the common depths and rock velocities, this time delay is on the order of a few tenths of a second. Results of non-linear finite difference calculations, while producing delay times greater than those

predicted by elastic theory, still produce delay times on the order of tenths of seconds (Mellman et al., 1980). As teleseismic short period recordings have a duration of >1 sec, the pP arrival is entangled with the direct P arrival and usually is not visible as a distinct phase. Thus, in modeling the resultant waveform we need to include the pP contribution. We will assume the pP arrival has the same shape as direct P. This assumption is simply that the upgoing and downgoing time functions are identical except for an amplitude scale factor. Fracturing of the rock above the explosion might cause the pP arrival to have a broader time function, thus delaying the peak amplitude of pP slightly beyond the time expected from the burial depth and rock velocity. However, it will be shown that resolving different source time parameters for pP is a very difficult task.

It is necessary to consider a range of t^* values. In the earliest attempts to model teleseismic seismograms, it was assumed that $t^* = 1$ sec and that t^* was constant for the teleseismic distance range ($\Delta \sim 30$ to 80 deg.). This value has been in popular use since then, if only because there was no compelling evidence for a different value. More recent work using digital short period instruments peaked at a higher frequency than the WWSSN short period (which is peaked at 1.4 hz) seems to indicate that t^* could be substantially lower than 1 (e.g., Mellman and Hart, 1980; Der, et al. 1979), perhaps 0.5-0.6, and in some cases values of

0.1-0.2 have been discussed. It is rather disturbing to have an order of magnitude uncertainty in a quantity that appears in an exponential, as the observed amplitudes depend upon t^* as,

$$A \sim \exp(-\pi f t^*)$$

Thus, at $f = 1$ hz., allowing the range $t^* = 0.1$ to $t^* = 1.0$ introduces a factor of ~ 17 uncertainty in the amplitude. As the amplitudes of the P-waves are used to determine the yield, clearly the value of t^* is of primary importance. These uncertainties in t^* also affect the determination of the other source parameters as well.

II. METHOD

As a large number of presumed underground nuclear events in the Soviet Union have been well recorded on the WWSSN short period instruments, a method has been developed which utilizes these photographically-recorded seismograms. The essential idea is that the short period waveforms can be entirely characterized by the peaks and troughs (unless there are obvious inflections). That is, the waveform can be reproduced to within the thickness of the photographic recording by using a cosine interpolation between the peaks and troughs (see Figure 1). The available independent data are the relative peak amplitudes and peak times. Thus, for the typical short period waveform with four peaks, we can represent the waveform with only eight independent numbers corresponding to the amplitudes and arrival times of those peaks (see Figure 3). This type of representation has also been used by Somerville, Wiggins, and Ellis (1976).

In previous studies, the time domain technique for determining the teleseismic time function of nuclear events was to "match" synthetic seismograms with the observed seismograms in a trial-and-error fashion (e.g., Burdick and Helmberger, 1979). Instead of applying this rather subjective method, we have used a formal waveform inversion based on the peak-trough data characterization (note that the "match" criteria is similar to that used when visually matching the synthetic to the data). Setting up the formal

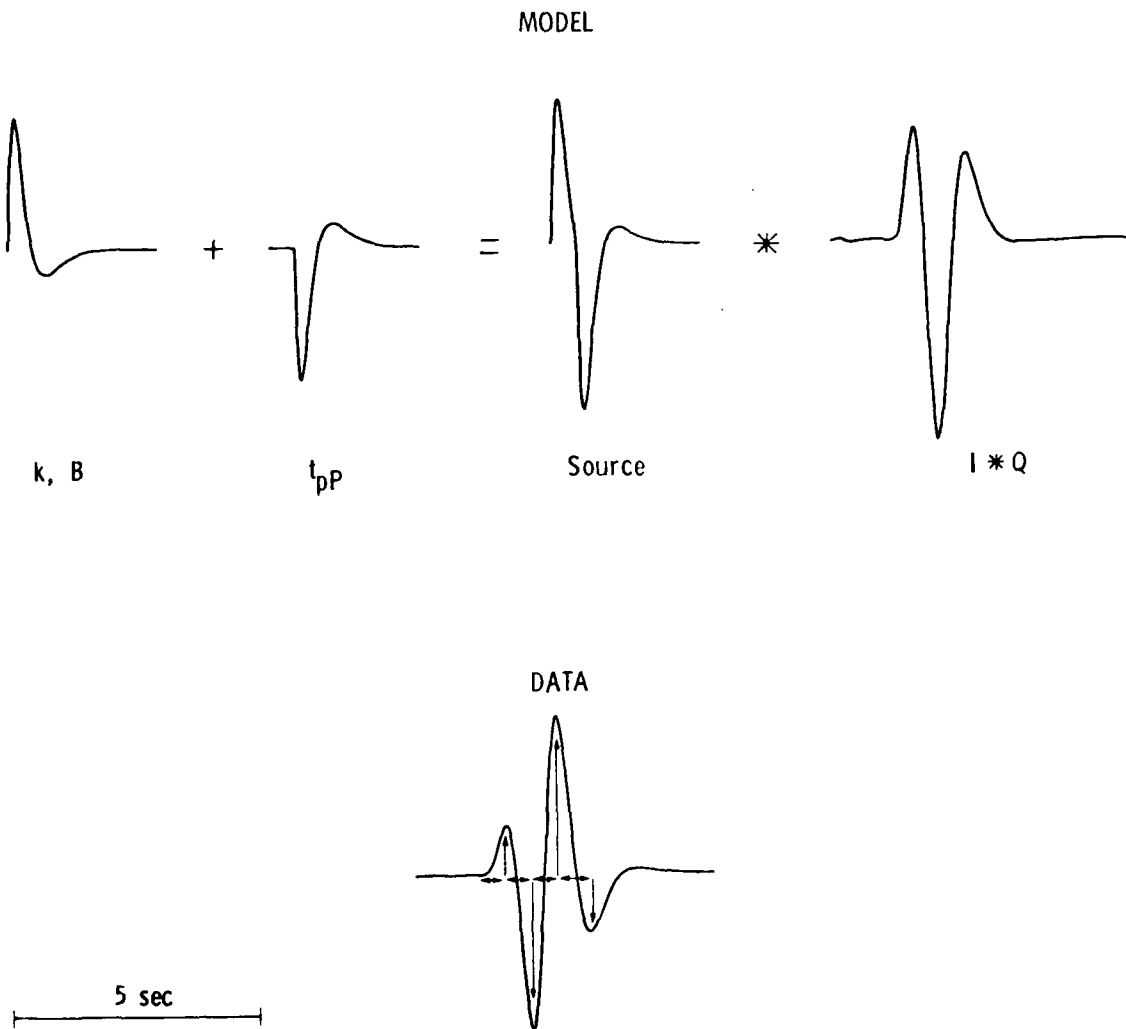


Figure 3. Synthetic seismograms are constructed by convolving the source time function with the instrument and Q operator. A typical source time function is shown, along with the instrument convolved with the Q operator for $t^* = 1$. The data and synthetic are then parameterized by the peak amplitudes and times (as shown in the lower portion).

inversion problem allows for an investigation of the uniqueness of the solution. The trade-off between the three parameters (k , B , t_p) which produce similar seismograms has not previously been well explored. Additionally, the method could potentially be used for the systematic estimation of source parameters.

In the time domain, the seismogram $S(t)$ is constructed as the convolution,

$$S(t) = I(t) * Q(t; t^*) * F(t; k, B) * D(t; t_p, R)$$

where I is the instrument, Q is the attenuation operator, F is the source time function, and D is the half-space Green's function (a delta function at $t = 0$ followed by a negative delta function at the pP delay time t_p), and R is the effective surface reflection coefficient which we initially take to be -1. In the teleseismic range, the earth response results only in a spreading factor, there are no significant waveshape changes at the periods of interest. In our procedure, we fix I and Q , then determine the function $F*D$ as parameterized by k , B , and t_p . Formally, as soon as we discretize $S(t)$ in the above relation there is no unique solution for the unconstrained function $F*D$. It is necessary to impose a smoothness condition on $F*D$. Notice however, that F is parameterized by just two variables, k and B , and, indeed, is itself a smooth function. Thus, although the source parameters occur in a nonlinear fashion in F , we might hope that the three source parameters could be determined uniquely.

As the parameters appear in a nonlinear fashion, we adopt the usual linearization procedure in formulating the problem. Given initial estimates for the parameters, we form the error vector $\underline{\varepsilon}$, $\underline{\varepsilon} = \underline{d} - \underline{S}(k, B, t_p)$, where \underline{d} is the data. If the error is unacceptable, we want to change \underline{S} to force $\underline{\varepsilon}^2$ toward zero,

$$\underline{0} = \underline{d} - (\underline{S} + \delta \underline{S})$$

then

$$\delta \underline{S} = \underline{\varepsilon}$$

To find the required parameter change, we expand the synthetic around the current parameter values,

$$\delta \underline{S} = \frac{d \underline{S}}{d p_j} \frac{\partial p_j}{\partial p_i} \Delta p_i + \dots$$

Ignoring the higher order terms, we then have

$$\frac{d \underline{S}}{d p_j} \frac{\partial p_j}{\partial p_i} \Delta p_i = \underline{\varepsilon}_i$$

a linear system of the form $Ay = b$, and with three parameters and eight data values, an overdetermined system.

After solving the above system, the new parameter values will be ${}_1 p = {}_0 p + \Delta p$. As the higher terms in $\delta \underline{S}$ have been ignored, and data errors lead to an incompatible system, it is likely that the error has not been reduced completely to zero, and ${}_1 \underline{\varepsilon} = \underline{d} - \underline{S}({}_1 p)$. Thus, we iterate with the same procedure to reduce ${}_n \underline{\varepsilon}$ to the desired level, dictated by the data variance. In most inversion procedures where there can be large numbers of parameters and data, one would select

different starting models (\underline{p}_0), and allow the method to iterate to test whether the procedure converges to the same solution. In our situation, given the small size of the system (8x3), it is feasible to "map out" the three dimensional parameter space, thereby examining the properties of convergence for synthetic data. One display method is to contour the modulus squared of the error vector as a function of the parameters,

$$\epsilon(\underline{p})^2 = \underline{d} - \underline{s}(\underline{p})^2$$

However, contouring the length squared error vector does not display the length of the parameter perturbation, particularly when damping is used. Hence, the properties of convergence are displayed here with "vectorgrams". A vectorgram plot the parameter perturbations as a function of the parameter values. At a particular \underline{p} , let $A_{ij} = ds_i/dp_j$, then solving the system $A_{ij}\Delta p_j = \epsilon_i$ we obtain $\Delta p_j = A_{ji}^{-1}\epsilon_i$. Thus at any \underline{p} we plot the associated $\underline{\Delta p}$, with the tail of the vector at \underline{p} and the head at $\underline{p} + \underline{\Delta p}$. We can then plot the $\underline{\Delta p}$ at network of values for \underline{p} . Figure 4 shows a vectorgram using synthetic data (in which the "true" solution is of course known). The three-dimensional network of parameter values samples k and B quite well, covering the range of 1 to 9 and 0 to 4 respectively, while only three values of t_p (0.4, 0.5, 0.6 sec.) are sampled. The limited sampling of t_p is adequate as Δt_p is well resolved everywhere, which is demonstrated in a later section.

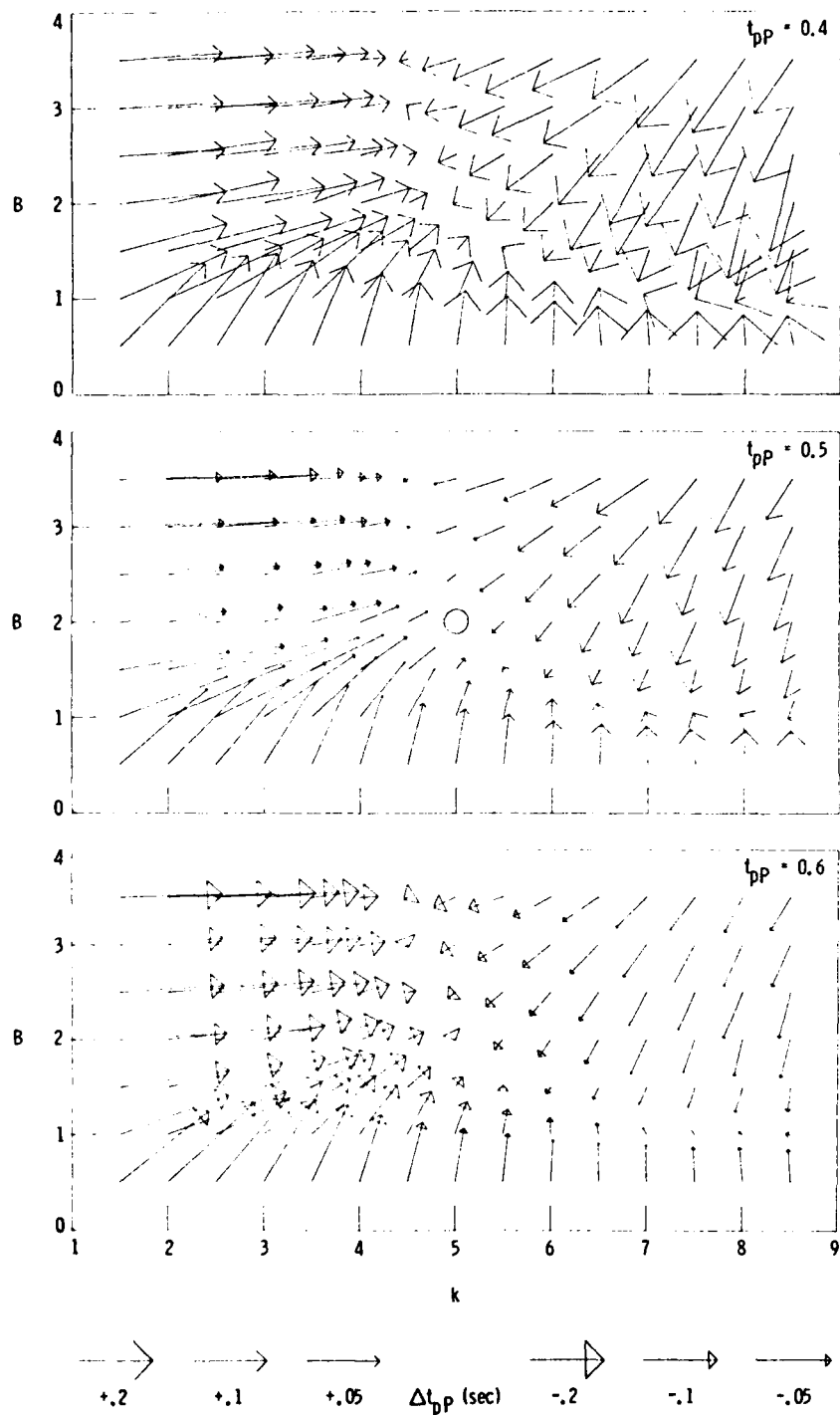


Figure 4. Vectorogram for synthetic data. The data are taken from a synthetic seismogram computed with the following parameters: $k=5$, $B=2$, $t_p=0.5$, and $t^*=1$. The vectorogram displays the parameter perturbations calculated at a network of (k, B, t_p) values, with 1% damping. Starting at initial values for k , B , and t_p , the vectorogram shows the path that the inversion procedure would follow.

III. RESULTS

3.1 Properties of the Inversion Method

There are several features in Figure 4 that persist for many of the cases that have been considered. One important feature in Figure 4 is that the method does converge to the "true" solution, if a suitable starting place is selected. If one starts with small values of k and B , the method proceeds directly toward the answer. Figure 5 is a sample inversion run starting with small values of k and B . However, when starting at any other corner of the k, B plane, the method would proceed to the "trough" and stop without reaching the "true" answer. This trade-off curve, which extends toward a larger k and a larger B from the correct solution, appears to represent an inherent nonuniqueness in the solution, and is present in all vectorgrams with artificial data for a variety of short-period instruments. To show that this trough is not an artifact of the inversion procedure, Figure 6 compares the synthetic seismogram for parameters (5.0, 2.0, 0.5) with two other synthetic seismograms computed with parameter values at either end of the trade-off curve, and indeed they are quite similar. Looking at the source description formula, the nature of this trade-off is not obvious. If we compare the spectral amplitudes of the source time functions (Figure 7), it would seem that the k, B trade-off combinations maintain the level of the high frequency slope relative to the low frequency level. It appears that the height of the spectral high due to the

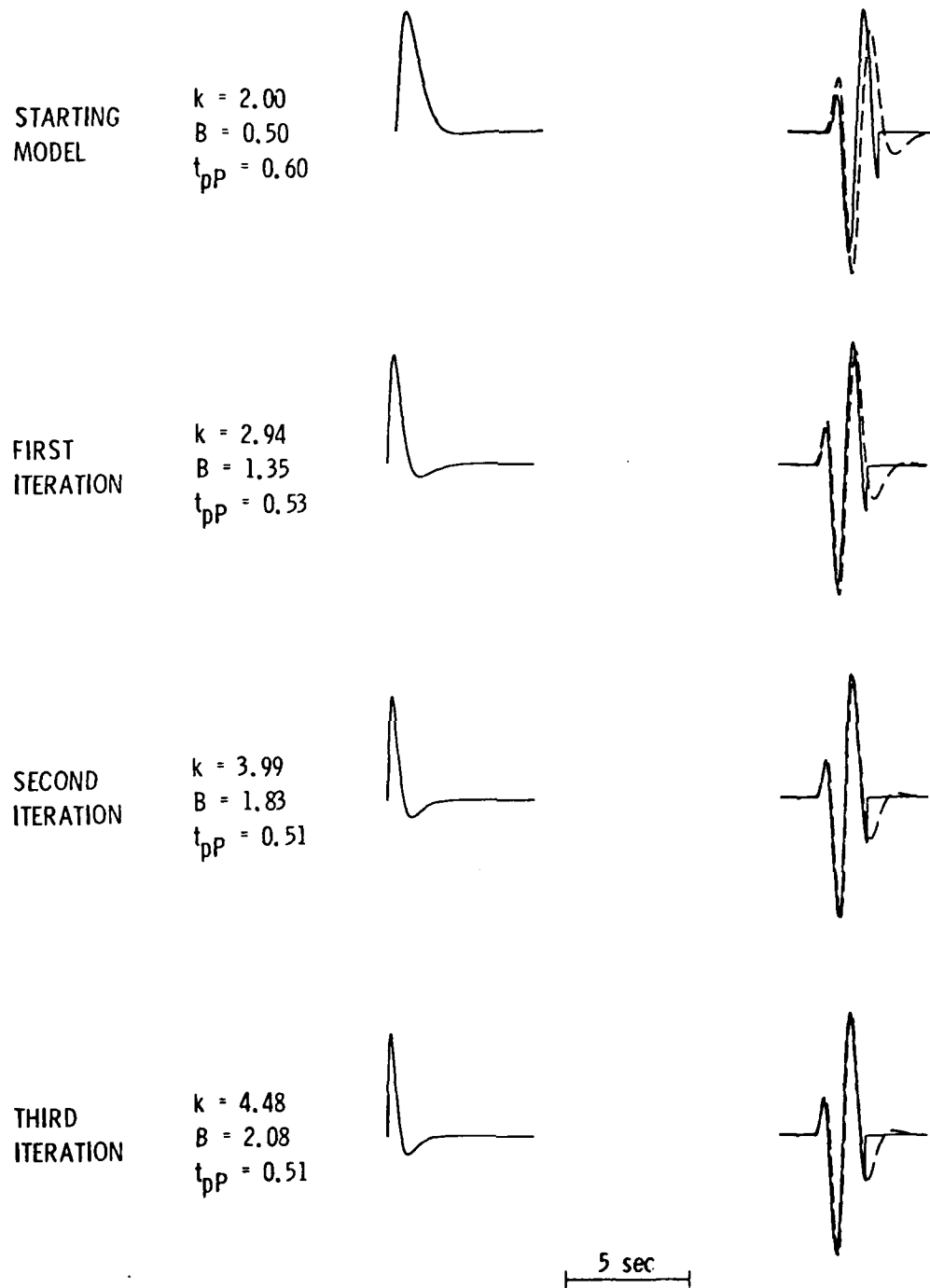


Figure 5. An inversion sequence for the synthetic data used in constructing the vectorgram in Figure 4. The source time functions and resultant synthetic seismograms are shown for the starting model and three iterations. The solid trace at each iteration is the "data" (computed with $k=5$, $B=2$, $t_{pP}=0.5$), and the dashed trace is the synthetic corresponding to the source parameters of that iteration. There is an excellent agreement after three iterations.

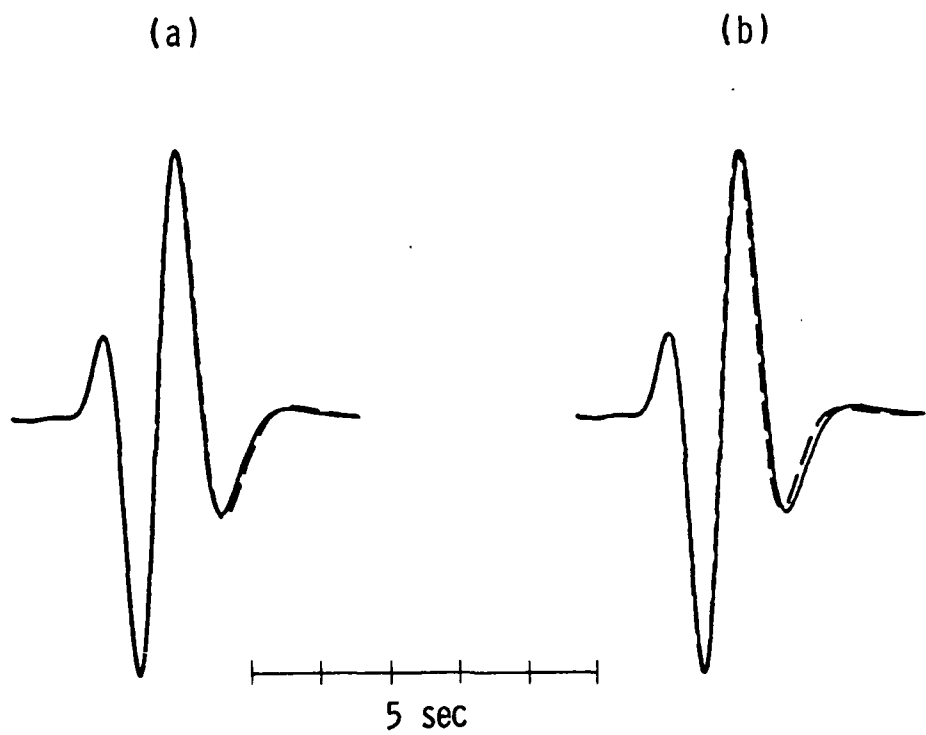


Figure 6. Comparison of synthetics along the trade-off curve, using the WSSNSP instrument with $t^*=1.0$ and $t_{pp}=0.5$ sec in all cases. The synthetic seismogram for $k=5$ and $B=2$ is shown in both (a) and (b) as the solid trace. The dashed trace in (a) is the synthetic seismogram for $k=4.4$ and $B=3.5$. The dashed trace in (b) is the synthetic seismogram for $k=6.5$ and $B=1.3$.

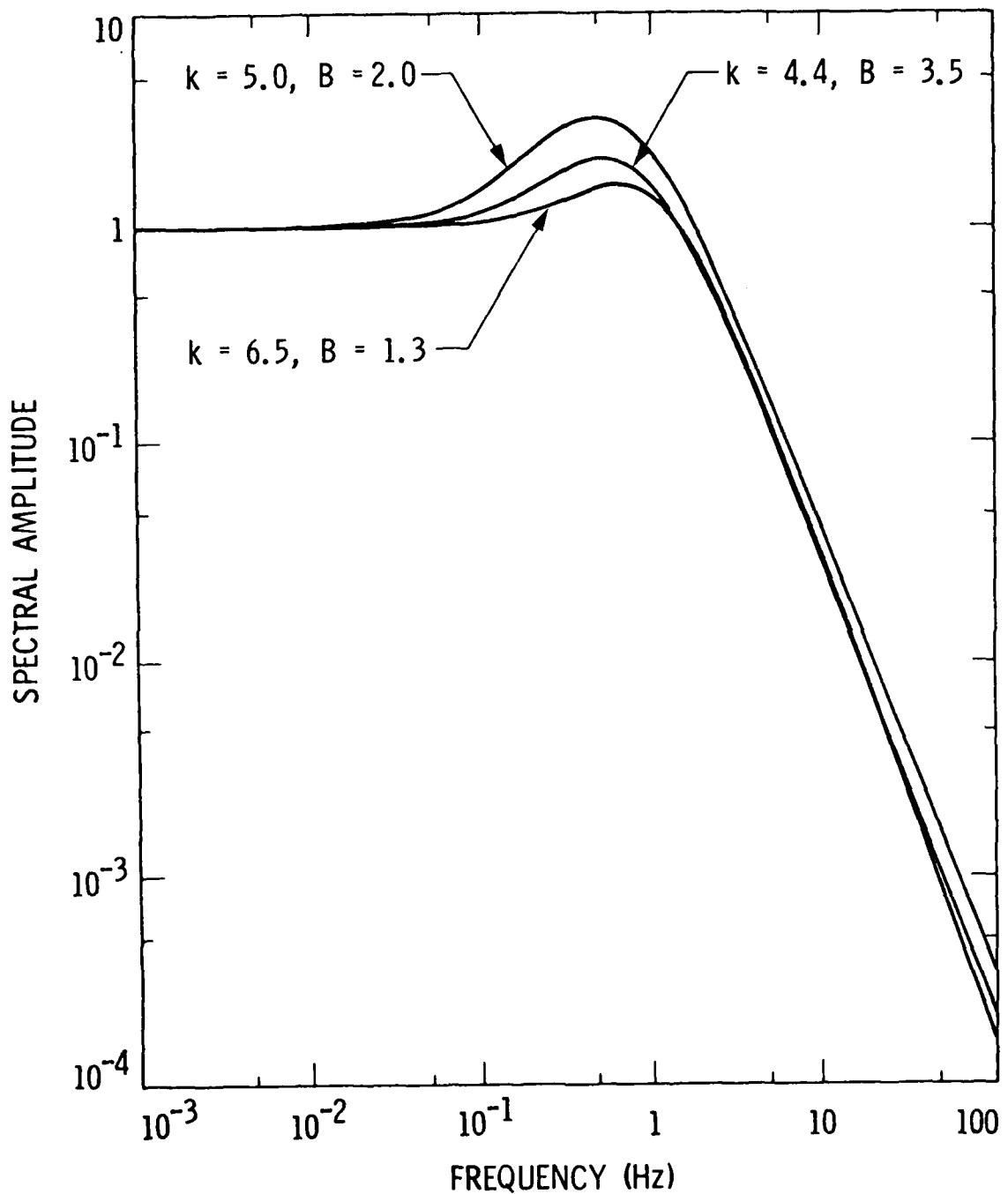


Figure 7. The spectral amplitudes for three different (k, B) combinations. These three combinations are on the trade-off curve in Figure 4. It appears that k, B values on the trade-off curve are characterized by maintaining the high frequency decay slope at the same level relative to the zero frequency level.

overshoot does not exert a strong influence on the waveforms. This may be partly due to the spectral null that is introduced at about this frequency by the pP arrival.

Based on other examples of synthetic data, we conclude that this trade-off curve is a persistent feature of this inversion technique, but that the "true" solution lies at the corner of the trade-off curve. Thus, starting with low values of k and B , then allowing the inversion technique to proceed should provide at least systematic estimates of the source parameters.

It was stated earlier that t_p is well resolved, in that the correct value of t_p is closely approximated after just one step from a large part of the k, B, t_p network. Once again, many different vectorgrams for different cases exhibit this feature. In this regard, it is instructive to plot the resolution matrices at each gridpoint. The resolution matrix, R , is

$$R = A^{-1}A$$

where A^{-1} is the particular inverse used. In the case of no damping and no data weighting, the LANCZOS (1961) inverse is,

$$A^{-1} = (A^T A)^{-1} A^T$$

With this definition R is the identity matrix, that is, all three parameters are resolved, the three diagonal elements equaling 1. However, the solutions are somewhat unstable. Moving to an adjacent gridpoint results in a significantly different Δp . It was found that a 1% damping gave the desired stability, resulting in the inverse,

$$A^{-1} = [A^T A + \epsilon \text{Tr}(A^T A)]^{-1} A^T$$

With this form of A^{-1} , R is no longer the identity matrix, and the parameters associated with a small eigenvalue will have a diagonal element between 0 and 1. The three diagonal elements; corresponding to three parameters k, B , and t_p ; are plotted as histograms at each gridpoint (Figure 8), with the top of each box corresponding to a value of 1. It is quite obvious that Δt_p is resolved everywhere, and this is typical for other t_p planes. There are two other important conclusions to be reached from Figure 8. One is that the value of B is only well resolved for small values of B , that is, the waveform "knows" whether $B = 0$ or $B > 0$, but beyond a certain limit the value of B is not well determined. Also, the value of k is well resolved for small k , up to $k \sim 5$. Beyond that, the value of k is poorly determined. This can be understood as for $k > 5$, the basic source function pulse width is < 0.5 sec., approximately the minimum value of any peak-to-peak time. Thus, in the limit of large k , the source function is basically a delta function compared to the teleseismic waveform (i.e., there would be negligible differences in the waveforms between $k = 20$ and $k = 30$). This is an inherent difficulty in characterizing the data by the peaks, very little information can be ascertained for periods substantially smaller than the period associated with the minimum peak time value. It should be pointed out that the quantitative values of these limitations is a function of the instrument response. The values discussed

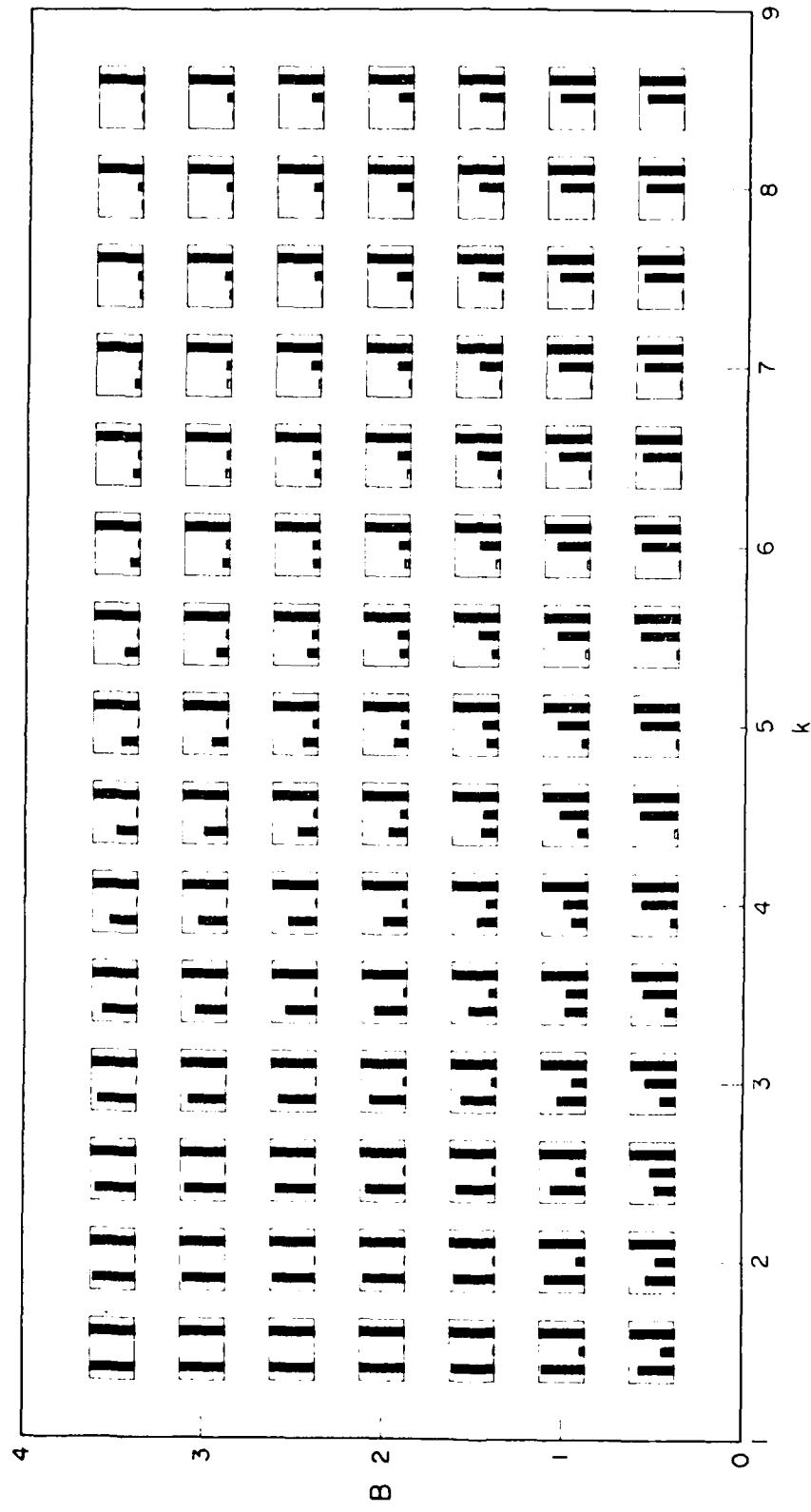


Figure 8. The diagonal elements of the resolution matrices for the network of (k, B) values, with $t=0.5$. At each (k, B) point, a histogram displays the size of the three diagonal elements, the first bar is for k , the second bar is for B , and the third bar is for t_B . The value at the top of each histogram is 1, i.e., well resolved, and the value at the bottom is 0.

above are those appropriate for the WWSSN short-period seismometer. A finer time resolution would be obtained from digital recordings of higher frequency instruments.

3.2 Source errors due to improper t^* and pP amplitude.

The vectorogram in Figure 4 is computed with $t^* = 1.0$, as is the synthetic used for data. Given the uncertainty in t^* , we would like to know what are the errors in the source parameters associated with an improper t^* value. Figure 9 shows an example where the synthetic data are for a $t^* = 0.8$, but we have assumed $t^* = 1.0$ in constructing the vectorogram. The form of the vectorogram is the same as Figure 4, though the "true" solution (at corner of the trade-off curve) has been shifted toward larger values of k and B , and t_p is modified slightly. Figure 10 is an example where the synthetic data are for $t^* = 1.2$, and the vectorogram is constructed with $t^* = 1.0$. The solution is then shifted toward lower values of k and B . Figure 11 shows the synthetic seismograms for different t^* 's and source parameter combinations, demonstrating that the inversion procedure does find a satisfactory match for quite a range of mismatch in t^* , over the k, B values considered.

Figure 12 shows the vectorogram for synthetic data computed with the proper t^* , but with the pP amplitude = - .8 while the vectorogram is constructed for pP amplitude = - 1. A shift similar to that due to an incorrect t^* is introduced. This may not be a severe problem as the theoretical

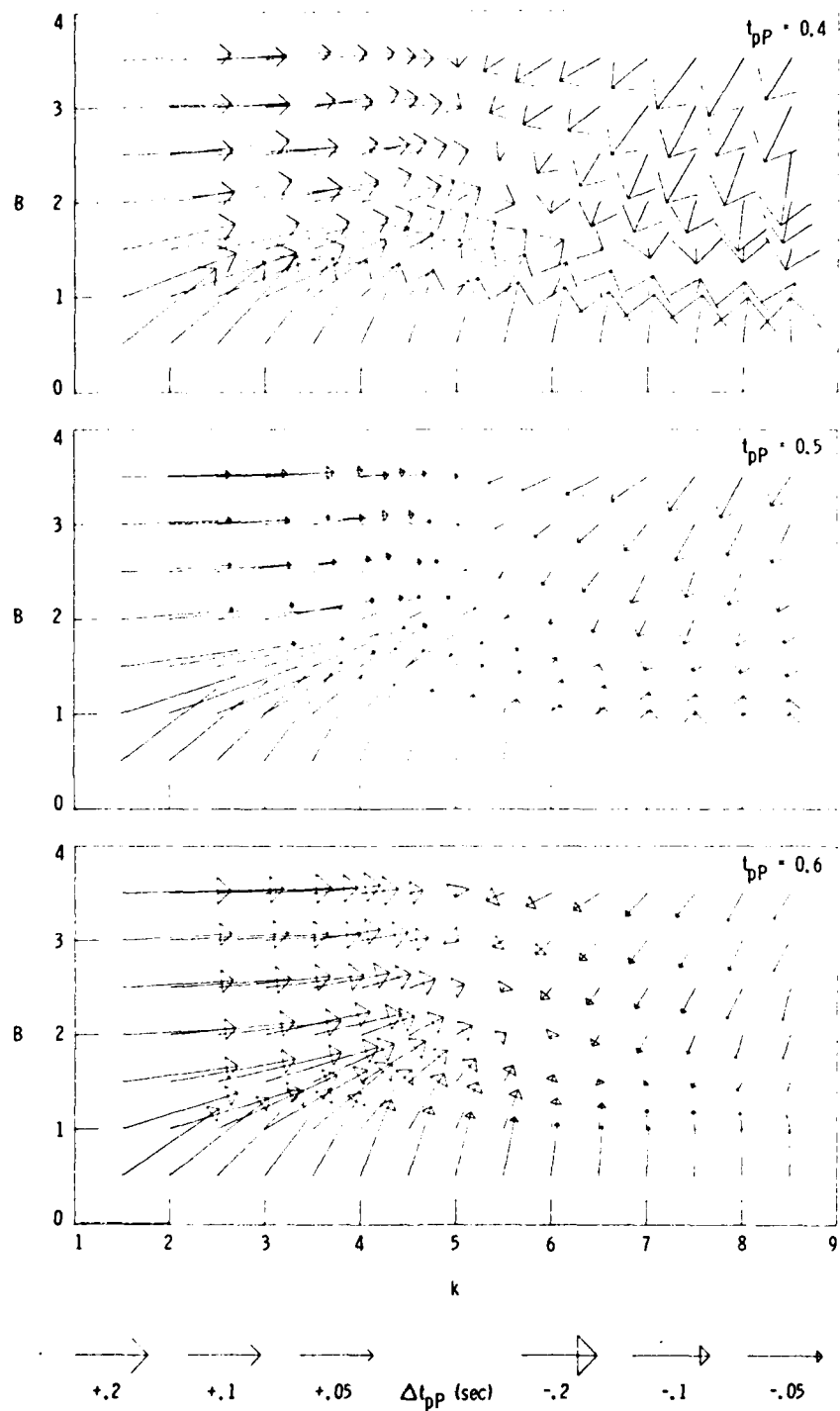


Figure 9. This vectorogram shows the error in parameter estimates introduced when the assumed t^* is incorrect. The synthetic data is computed for $k=5$, $B=2$, $t_p=0.5$ and $t^*=0.8$. The vectorogram is constructed assuming $t^*=1.0$. Notice that the "true" solution has been shifted from $k=5$ and $B=2$.

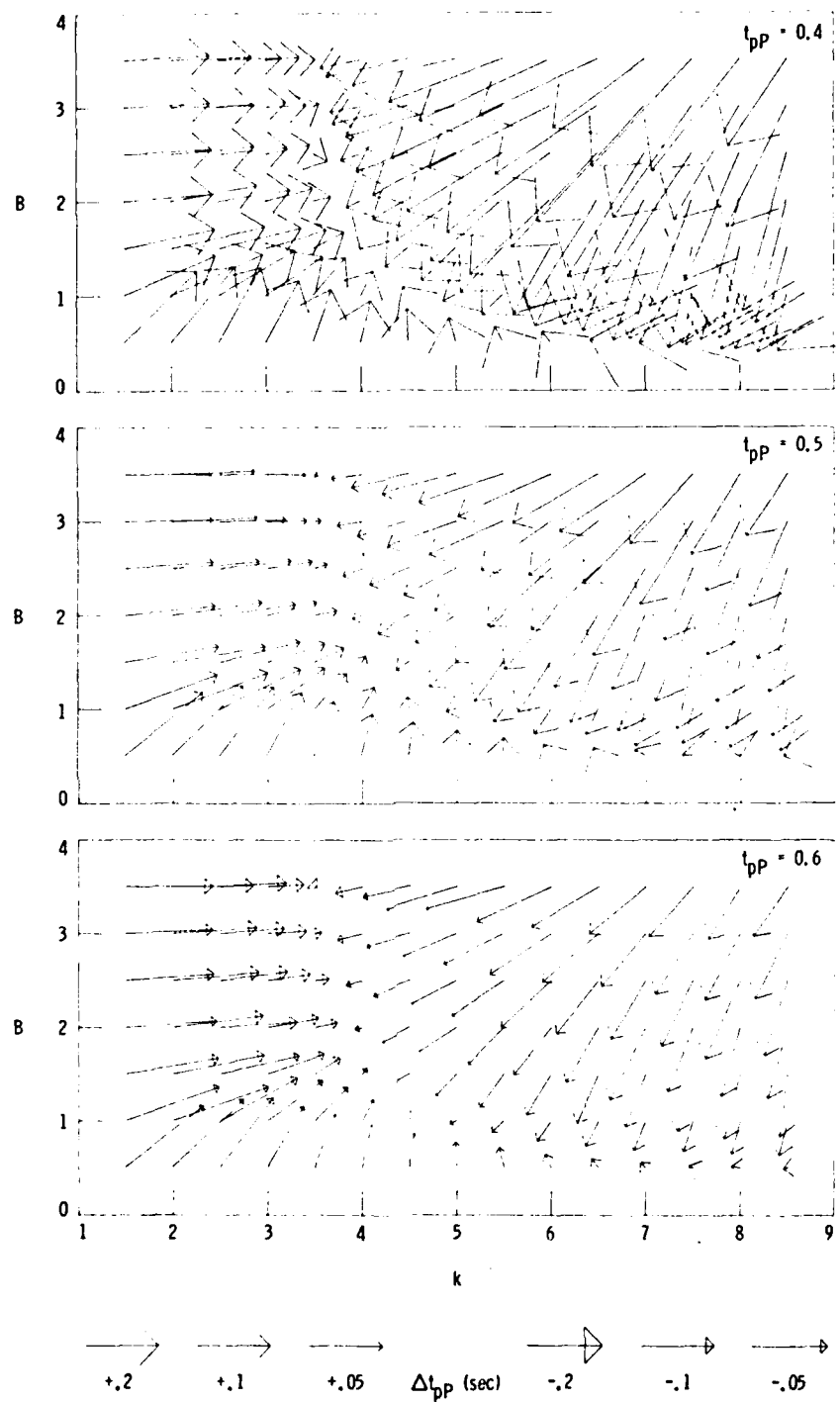


Figure 10. This vectorogram shows the shift in parameter estimates with an incorrect t^* value. The synthetic data is computed for $k=5$, $B=2$, $t_p=0.5$, and $t^*=1.2$, while the vectorogram is constructed assuming $t^*=1.0$.

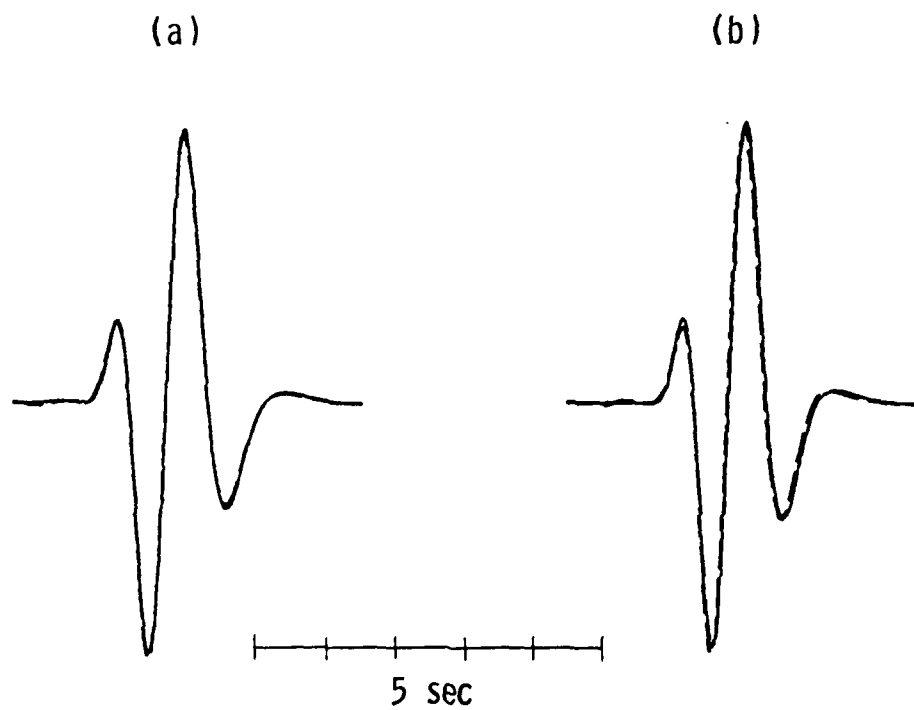


Figure 11. Comparison of synthetic seismograms with different values for t^* . In (a), the solid trace is computed for $t^*=0.8$, $k=5$, $B=2$, and $t_{pp}=0.5$, while the dashed trace is for $t^*=1.0$, $k=6.37$, $B=2.3$, $t_{pp}=0.45$. In (b), the solid trace is computed for $t^*=0.6$, $k=5$, $B=2$, and $t_{pp}=0.5$, and the dashed trace is for $t^*=1.0$, $k=9.5$, $B=4.5$, and $t_{pp}=0.40$.

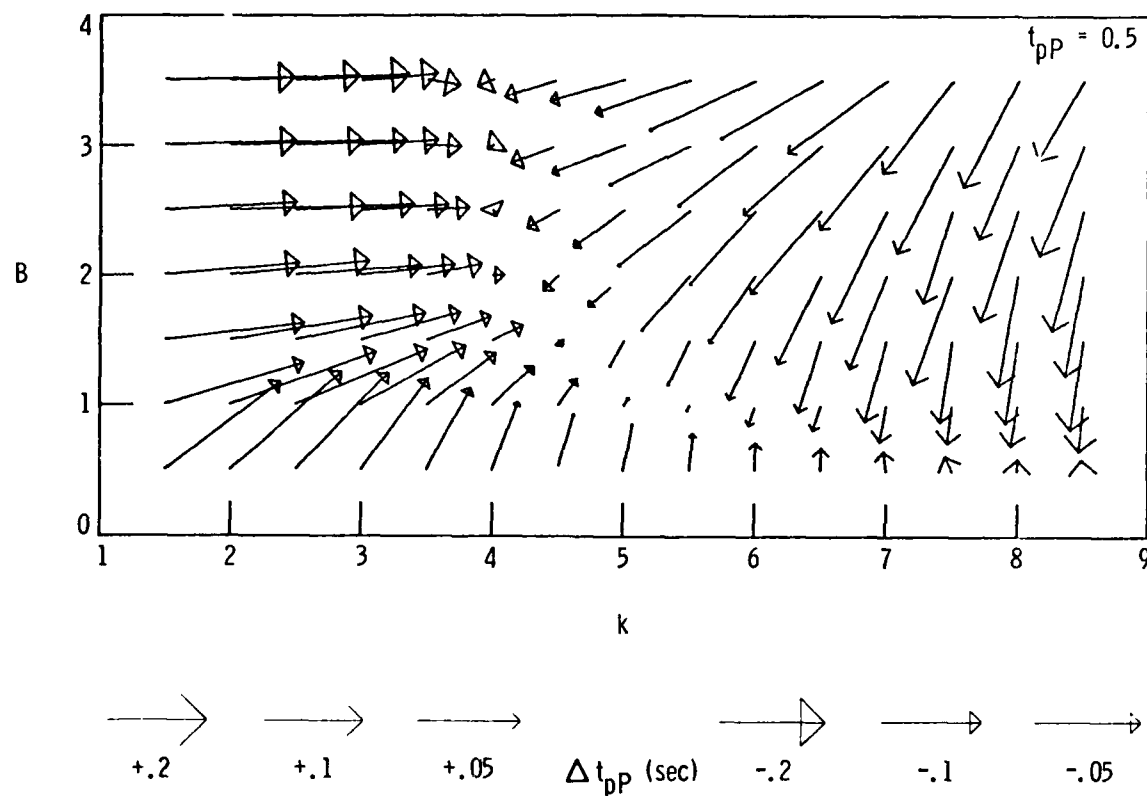


Figure 12. This vectorogram shows the shift in parameter estimates when the pP amplitude is incorrect. The synthetic data is computed with $k=5$, $B=2$, $t_p=0.5$, $t^*=1.0$, and pP amplitude=-0.8, while the vectorogram is computed for pP amplitude=-1.0 (the correct t^* value is assumed).

modeling indicates that a pP amplitude $\zeta \sim .85$ is adequate for many cases and this value could be used as the standard procedure. Regarding the possibility of allowing a different source function for pP, it seems clear from the resolution discussion that these parameters would not be resolved in general.

3.3 Results for Western Kazakh Test Site

Thus far, we have considered only error free data. In using real data there are two basic sources of noise; intrinsic record noise and waveform changes due to converted phases as discussed earlier. We can improve the signal to record noise ratio by selecting larger events to model. However, the converted phases (frequently referred to collectively as receiver structure) will persist. To gain some insight into the waveform scatter, three events (Dec. 6, 1969; Dec. 12, 1970; Dec. 23, 1970) which occurred in the Western Kazakh region were examined. These presumed explosions were located quite close to each other and the estimated yields range from 100 to 240 kt. (Dahlman and Israelson, 1977). When using all of the North American WWSSN stations the total scatter in the waveforms is quite large, though the peak times are in fair agreement, the scatter in peak amplitudes is distressing, particularly the fourth peak. Directly comparing the waveforms quickly isolates the clean or relatively transparent stations. The data vector is then formed by averaging together the peak

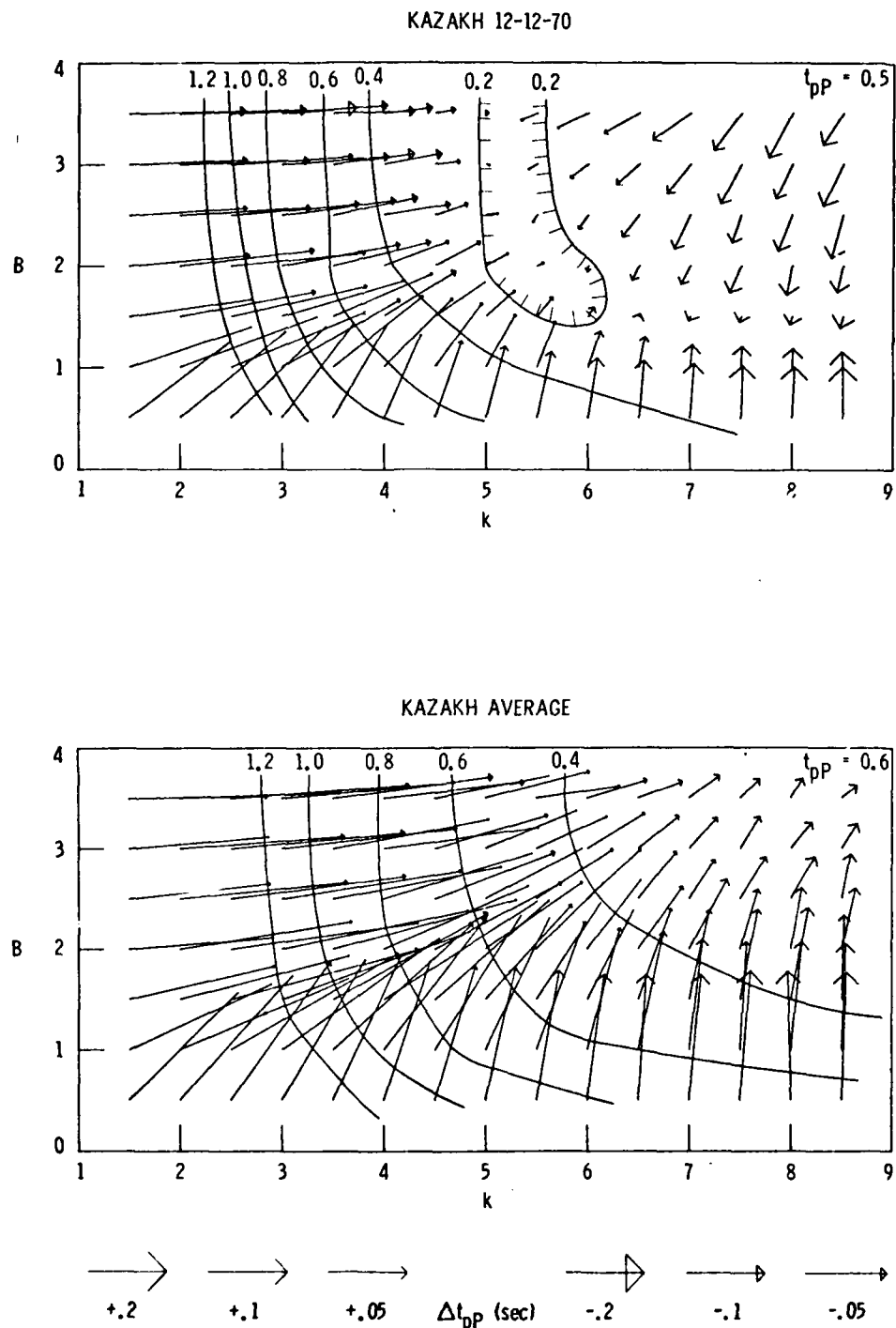


Figure 13. Two vectorgrams for two different averages of the data from events in Western Kazakh. The modulus of the error vector is contoured.

values from only a few of the best stations. Figure 13 shows two vectorograms for two different averages, one for the event of Dec. 12, 1970 and another for the combined average. A t^* of 1 was used in both cases. In the top vectorogram, the data produces a pattern quite similar to those of the synthetic data discussed earlier. The tradeoff curve is apparent and we could immediately choose the best solution at the corner of the trade-off curve ($k \sim 5.5$, $B \sim 2.0$, $t_p = 0.5$). The data vector used for Kazakh average is quite similar to that for Kazakh 12-12-70, the most significant difference being the peak value for the fourth peak, and yet the trade-off structure has disappeared and the vectors point off to the upper right-hand corner. In this situation it is important to consider the data errors. The contours in Figure 13 refer to the modulus of the error vector. In these units, a scatter in the peak times of 0.05 sec and of $\sim 10\%$ in the relative peak amplitudes gives an error modulus of ~ 0.4 , and we cannot expect the inversion to reduce the error much below this level. The closed 0.2 contour for Kazakh 12-12-70 requires the peak times to be within ~ 0.03 sec. and the amplitudes to be matched to $\sim 5\%$. Although there is no closed contour for Kazakh average, it would be reasonable to stop the inversion procedure at the 0.4 contour. In this case, it is of no great concern that there is no closed contour as this is probably due to the data scatter causing incompatibility. In this regard, the presence of the trade-off curve for Kazakh 12-12-70 might be fortui-

tous as opposed to better data quality. Figure 14 shows an inversion run using the Kazakh 12-12-70 data, and clearly a good fit is obtained after three iterations, though it has not yet progressed to the trade-off curve corner.

To quickly consider other t^* values, Figure 15 plots a vectorogram using the Kazakh 12-12-70 data and a $t^* = 0.6$. As expected, the source parameters move to a smaller k and slightly smaller B , the trade-off curve is present, and the mismatch acceptable. Lowering the t^* moves the source parameters into the region of resolution. Also note that t_p appears to be well resolved in these cases.

3.4 Inversion using SRO short period instruments

To extend the resolution of the source time parameters it is necessary to use seismograms with a higher frequency content. The SRO short period instrument is peaked at ~ 2.5 hz., in contrast to the ~ 1.3 hz. peak of the WWSSN instrument. Therefore, we might expect to increase the resolution with the SRO instrument. Also, the SRO is digitally recorded producing less ambiguity in determining the peaks (indeed ultimately we may wish to use more than just the peaks). To demonstrate that the basic properties of the inversion method apply when using the SRO instrument, Figure 16 shows the vectorogram for synthetic data with $t^* = 1.0$. Notice that t_p is slightly less stable than for the WWSSN instrument. Figure 17 plots the diagonal elements of the resolution matrices for $t^* = 1.0$. It is somewhat discour-

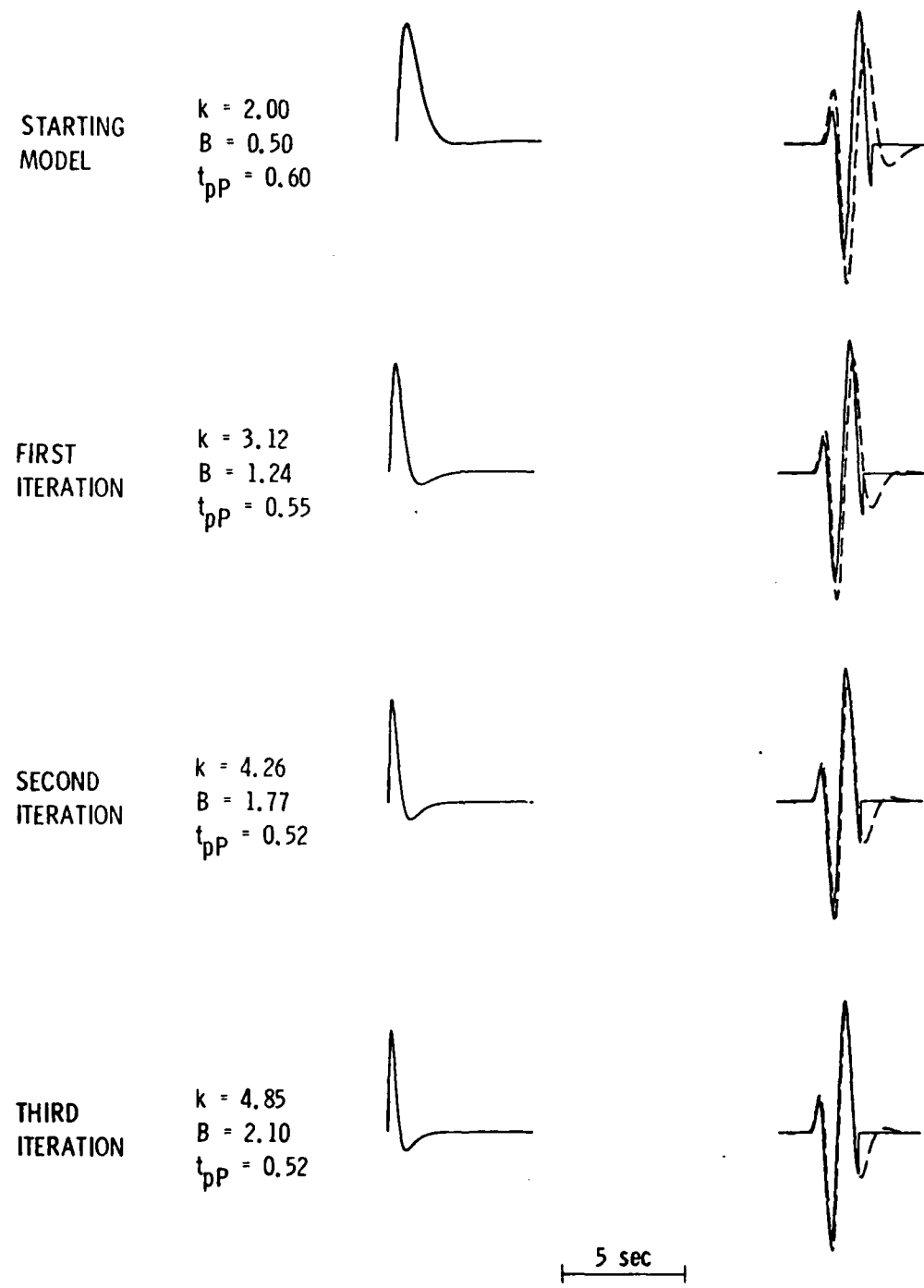


Figure 14. An inversion sequence for the Western Kazakh event of 12-12-70. As in Figure 5, the source time functions are shown on the left and the data (solid trace) and synthetic (dashed trace) are shown on the right. An acceptable match is obtained after three iterations.

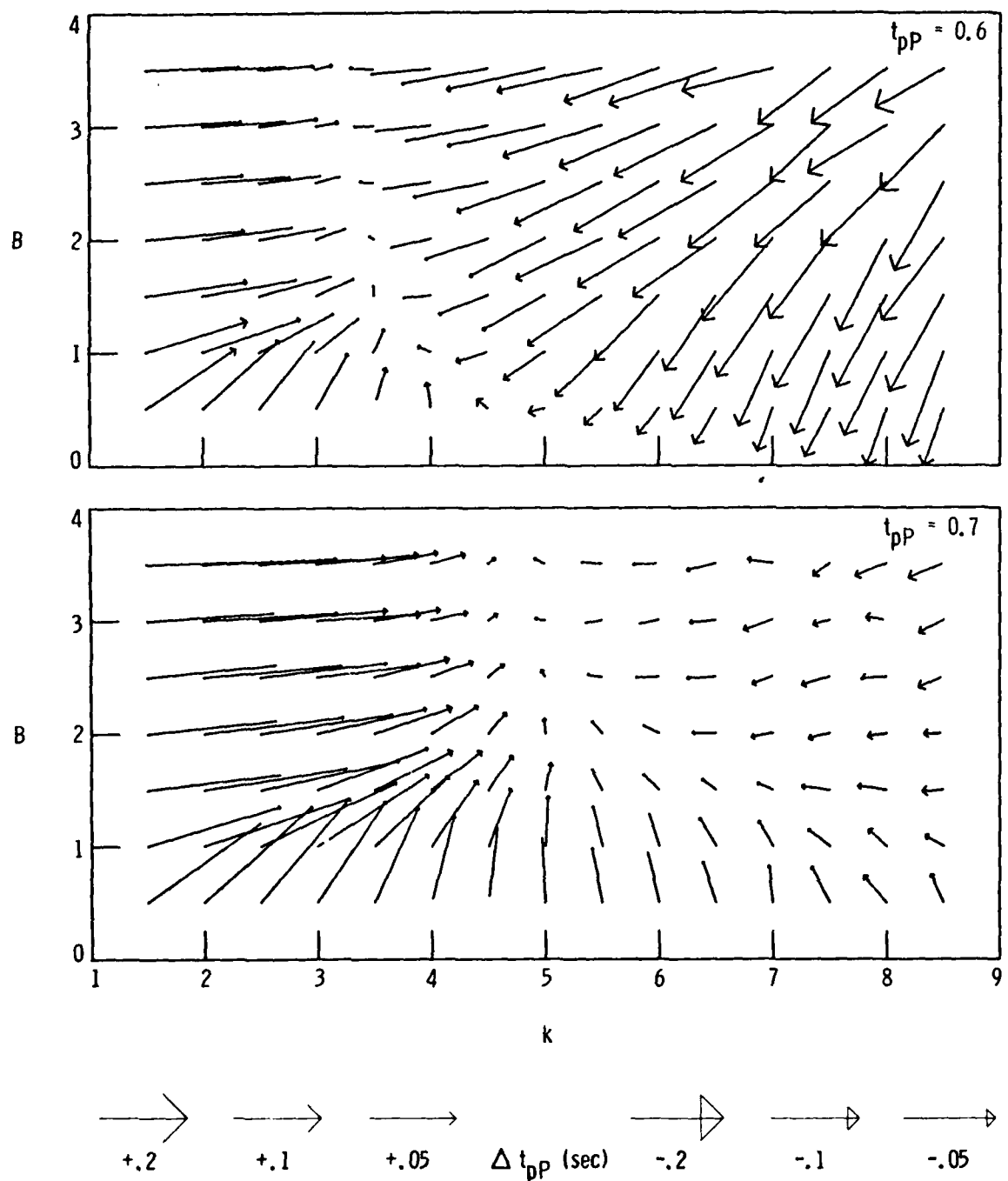


Figure 15. The vectorogram for the 12-12-70 Western Kazakh event computed with $t^*=0.6$.

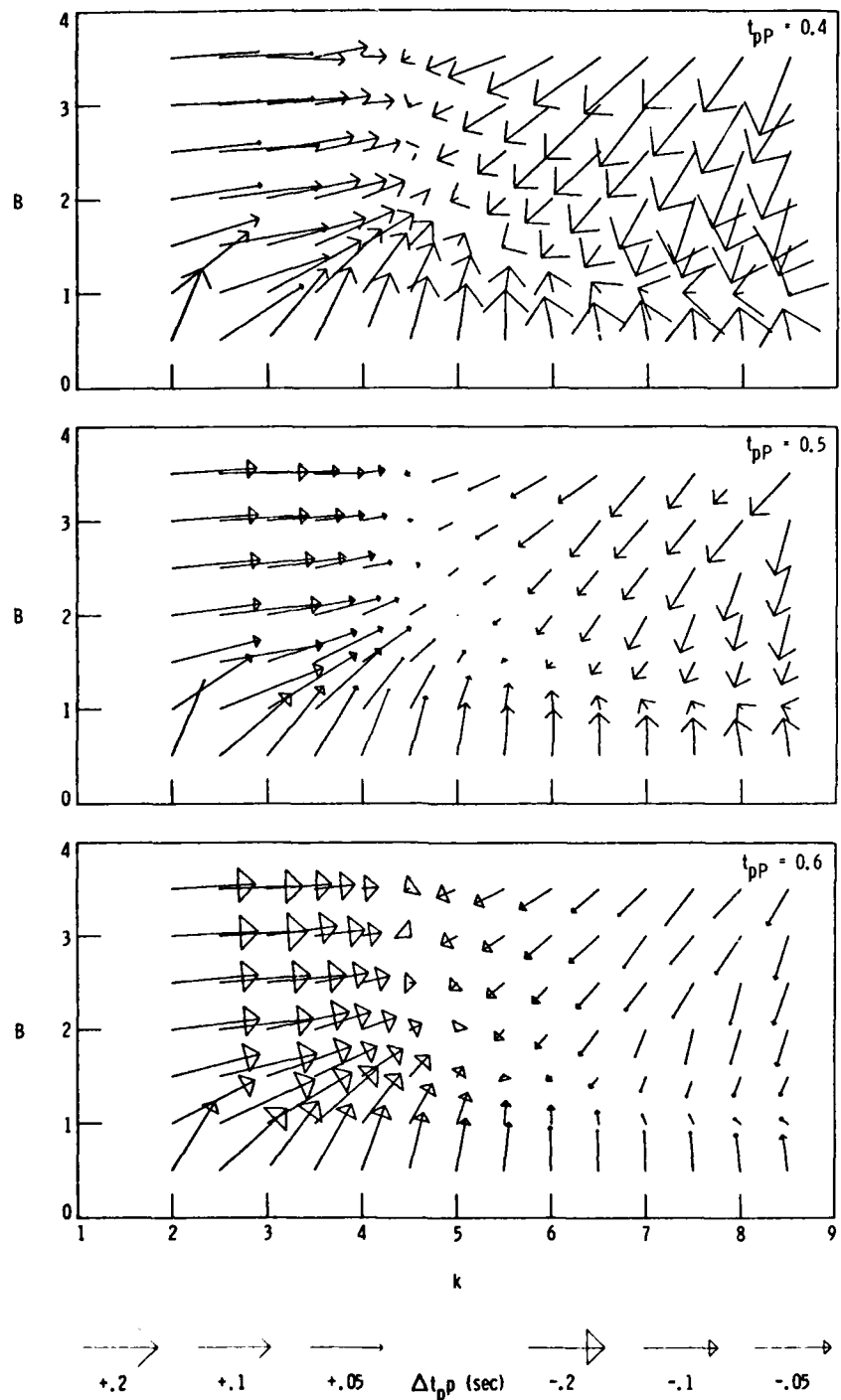


Figure 16. A vectorogram for synthetic data using the SRO short period instrument. The synthetic data is computed with $k=5$, $B=2$, $t_p=0.5$, and $t^*=1.0$. Notice that the basic structure is similar to that when using the WWSSN short period instrument.

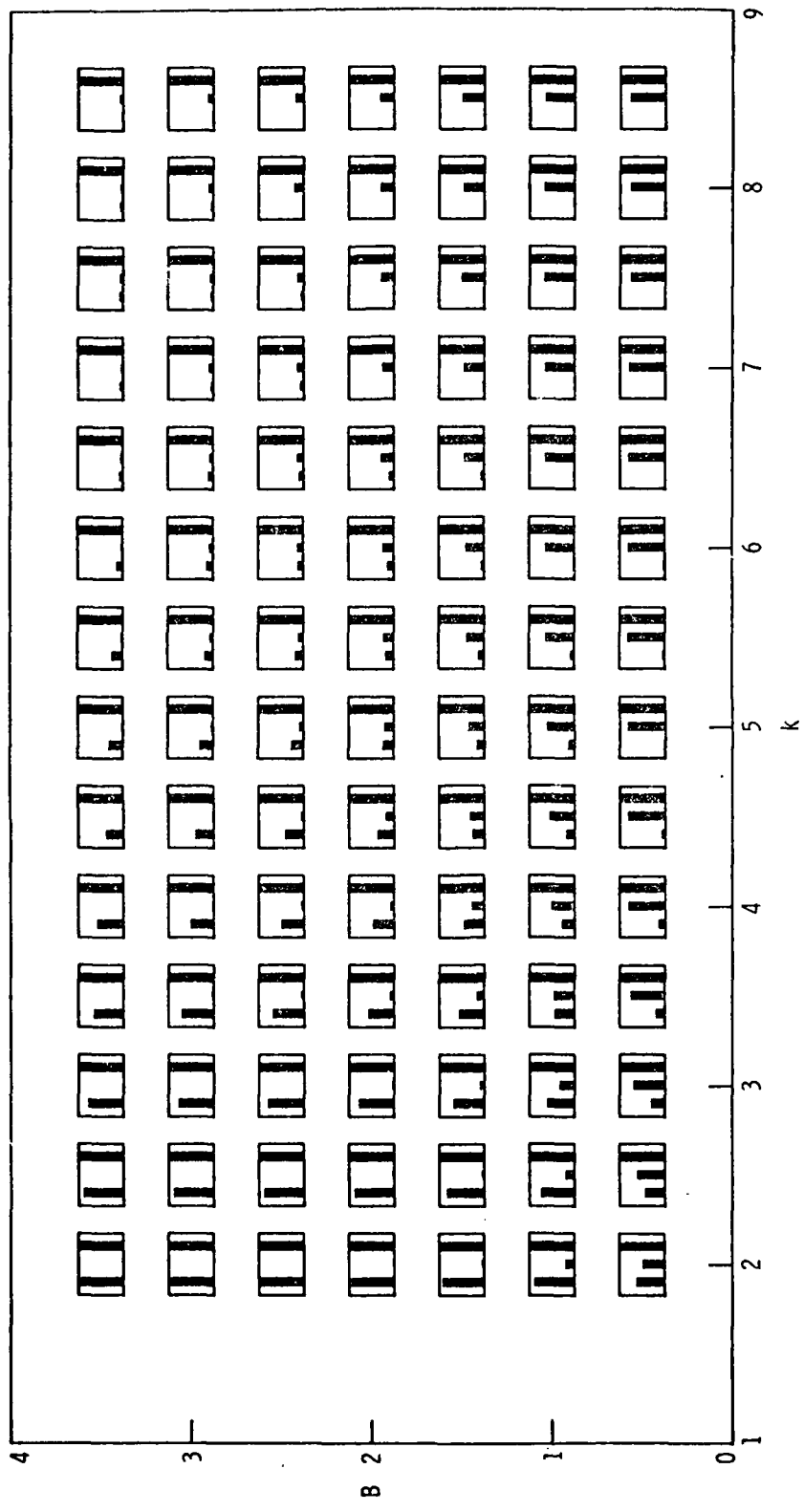


Figure 17. The diagonal elements of the resolution matrices for the SRO short period instrument, computed for $t^*=1.0$. As in Figure 8, each histogram depicts the resolution of the three parameters; k , B , and t_p , ranging from 0 to 1.

aging that we have not increased the resolution substantially, but this is verified as the SRO synthetics for $t^* = 1.0$ have peak times similar to the WWSSN synthetics. Clearly, the broad attenuation operator for $t^* = 1.0$ is limiting the resolution.

SRO data at several stations has been examined, and CTAO was chosen as one of the clean stations recording events from the Semipalatinsk area. When attempting to model the CTAO seismograms, it was found that $t^* = 1.0$ was not acceptable, as the peak to peak times of the synthetic seismograms were too long, even as k became quite large and t_p became quite small. Thus, one is compelled to use a lower t^* to produce synthetics with the appropriate pulse widths. Though it is difficult to determine exactly what value of t^* is appropriate, $t^* = 0.4$ appeared to be adequate for the seismograms considered. Another problem encountered was the value of the pP amplitude. Testing various values, the most compatible amplitude is -1.3. This is a bit difficult to reconcile, and the present interpretation is that this value includes a converted phase.

We have divided the events recorded by CTAO into two categories based upon size. Recalling the earlier discussion on source parameter scaling, it would be interesting if we could resolve such differences at an individual station. The events that will be considered are: 6-23-79 relative amplitude = 246, 6-11-78 relative amplitude = 128, and 8-4-79 relative amplitude = 215. As 6-23-79 is only a

factor of 2 larger than 6-11-78, we would expect that the value of k for 6-23-79 will be smaller by only $\sim 20\%$. As the distortion in the fourth peak is too large to ignore, the fourth peak amplitude and time have been given the weight of 0.01. Figure 18 shows the k, B paths followed by the different events. It appears that the smaller 6-11-78 event consistently prefers a slightly larger value for k and B as the iterations proceed. For example, starting at (2.0, .25, .5); after two iterations the 6-23-79 k value is $\sim 12\%$ smaller than the 6-11-78 value, after four iterations is $\sim 14\%$ smaller, and after five iterations it is $\sim 15\%$ smaller. These values are roughly consistent with the expected difference based on the simple scaling argument, though we cannot place a strong emphasis on this result until we understand the causes of the mismatch at CTAO.

Perhaps of more interest is t_p . Figure 19 plots the t_p values for the three events, and despite the oscillatory behavior there appears to be a resolvable difference in the pP time for 6-11-78, in the direction consistent with a shallower depth of burial for the smaller event. Figure 20 shows the inversion results, with the final time functions and synthetics for the two events; 6-23-79 and 6-11-78, recorded at CTAO. The differences in the seismograms are subtle, but can be seen with the aid of a ruler.

Concluding this preliminary investigation of SRO seismograms, some of the source to receiver combinations require a $t^* < 1$ to match the peak to peak times, and using the

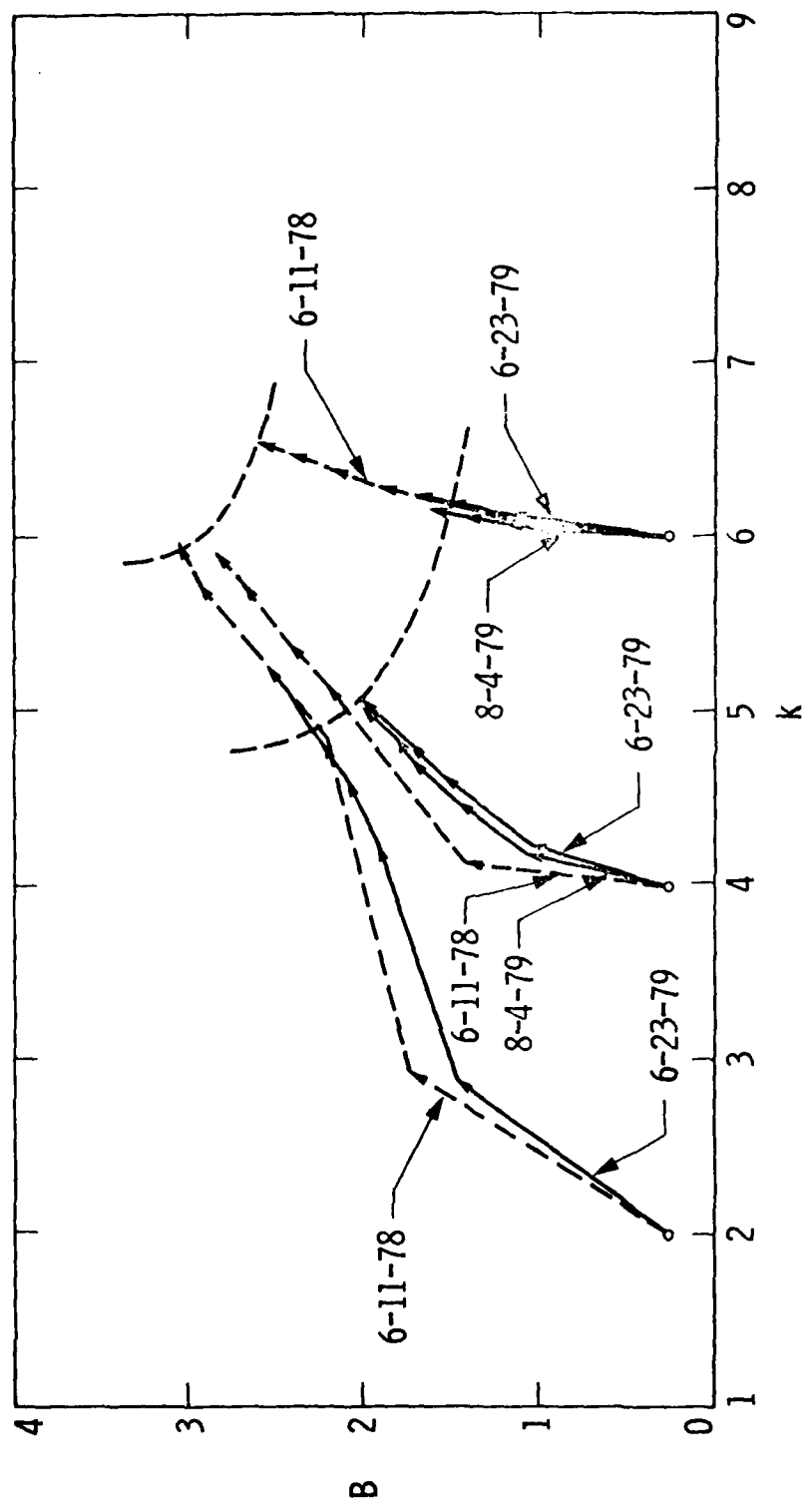


Figure 18. The (k, B) paths followed by the inversion procedure. The data used are three events, 6-23-79, 6-11-78, and 8-4-78, recorded by the SRO short period station, STAO. The t^* value is 0.4. Different starting models are used. The parameter estimates for 6-11-78 are consistently different than for 6-23-79 and 8-4-78.

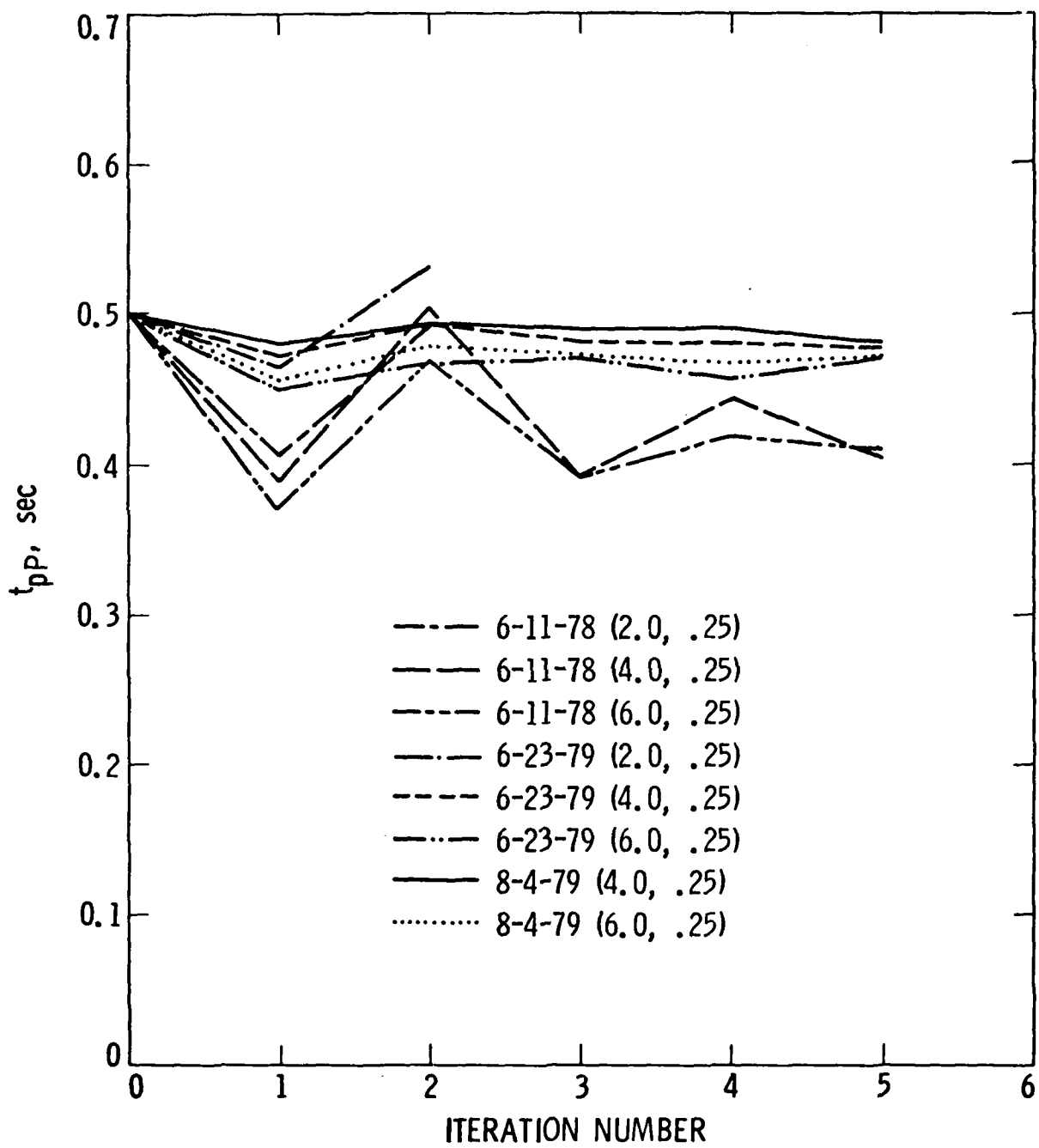
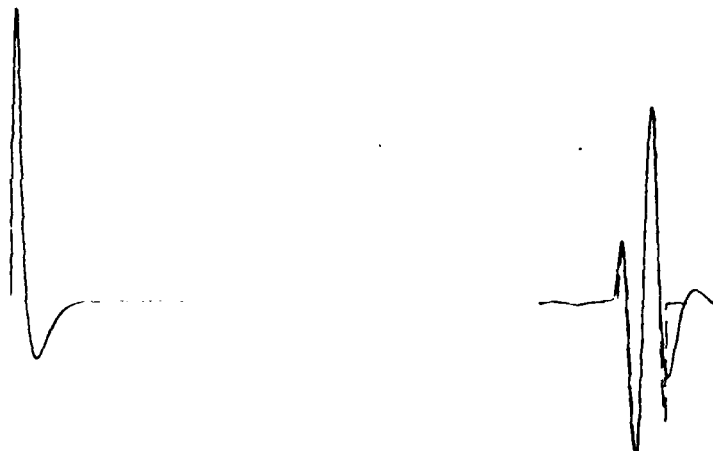


Figure 19. The t_{pp} paths followed by the inversion procedure when using the same events, station and starting models as in Figure 18. The value of t_{pp} for 6-11-78 is consistently lower than for 6-23-79 and 8-4-79.

(a)

INVERSION RESULT FOR 6-23-79, CTAO



(b)

INVERSION RESULT FOR 6-11-78, CTAO

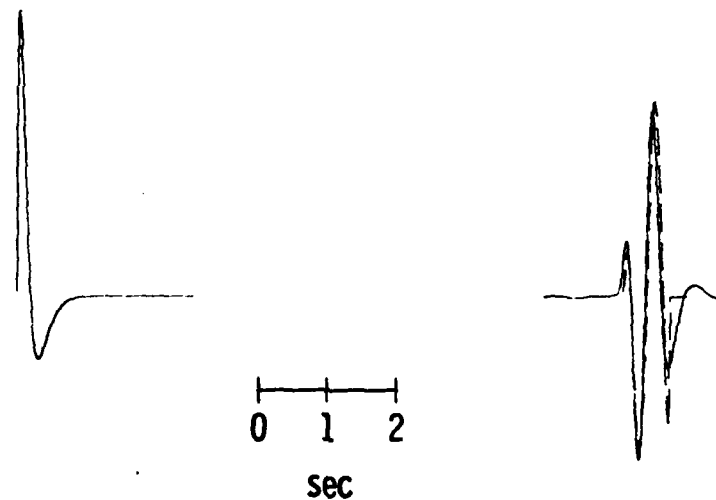


Figure 20. Inversion results for the two events: (a) 6-23-79 and (b) 6-11-78, recorded by the CTAO SRO short period instrument (the solid trace in (a) and (b)). With initial values of $k=2$, $B=2.5$, and $t_{pp}=0.5$ sec, the time functions and synthetics (dashed trace) after five iterations are shown. The source values for (a) are $k=5.1$, $B=3.1$, and $t_{pp}=0.41$. A $t^*=0.4$ and surface reflect coeff=-1.3 were used.

records at CTAO, there is a suggestion that the relative value of k between different events might be resolvable to $<10\%$, and the value of t_p might be resolvable to $<.05$ sec.

REFERENCES

Burdick, L.J. and D.V. Helmberger, Time functions appropriate for nuclear explosions, Bull Seism. Soc. Am., 69, p. 957, 1979.

Dahlman, O. and H. Israelson, Monitoring Underground Nuclear Explosions, Elsevier Scientific Publishing Company, Amsterdam, 440 pp., 1977.

Der, Z.A., T.W. McElfresh, C.P. Mrazek, D.P.J. Racine, B.W. Barker, A.H. Chaplin and H.M. Sproules, Results of the NTS experiment, Phase 2, SDAC-TR-78-4, Teledyne Geotech, Alexandria, VA, 1979.

Haskell, N.A., Analytic approximation for elastic radiation from a contained underground explosion, J. Geophys. Res., 72, p. 2583, 1967.

Lanczos, C., Linear Differential Operators, D. Van Nostrand, London, 564 pp., 1961.

Mellman, G.R., G.M. Lundquist, S.K. Kaufman, D.M. Hadley, R.S. Hart and C.A. Salvado, Comparisons of predicted far-field seismograms with observations of selected underground explosions, SGI-R-80-032, Sierra Geophysics, Inc., Arcadia, CA, 1980.

Mellman, G.R. and R.S. Hart, Review of Magnitude/Yield Estimation Preliminary Report, SGI-R-80-017, Sierra Geophysics, Inc., Arcadia, CA, 1980.

Somerville, P.G., R.A. Wiggins and R.M. Ellis, Time-domain determination of earthquake fault parameters from short-period P-waves, Bull. Seism. Soc. Am., 66, p. 1459, 1976.

von Seggern, D. and R. Blanford, Source time functions and spectra for underground nuclear explosions, Geophys. J. R. Astr. Soc., 31, p. 83, 1972.